

RESEARCH ARTICLE

10.1002/2014JC010378

A semianalytical model for sheet flow layer thickness with application to the swash zone

Thijs Lanckriet^{1,2} and Jack A. Puleo¹¹Center for Applied Coastal Research, Department of Civil and Environmental Engineering, University of Delaware, Newark, Delaware, USA, ²Now at International Marine and Dredging Consultants NV, Antwerp, Belgium

Key Points:

- Generalized semianalytical model for sheet flow layer thickness developed
- Model validated against oscillatory flow tunnel and swash zone measurements
- Bore turbulence is likely cause of intense sheet flow at the onset of uprush

Supporting Information:

- Readme
- Figure S1

Correspondence to:

T. Lanckriet,
thijs.lanckriet@imdc.be

Citation:

Lanckriet, T., and J. A. Puleo (2015), A semianalytical model for sheet flow layer thickness with application to the swash zone, *J. Geophys. Res. Oceans*, 120, 1333–1352, doi:10.1002/2014JC010378.

Received 9 AUG 2014

Accepted 19 JAN 2015

Accepted article online 27 JAN 2015

Published online 25 FEB 2015

Abstract A new semianalytical model for the time-dependent thickness of the sheet flow layer that includes the effects of pressure gradients, bed slope, boundary layer growth, and bore turbulence is presented. The shear stress and boundary layer growth are computed using the boundary layer integral method. The model is expressed as two coupled ordinary differential equations that are solved numerically given a prescribed time series of free-stream velocity, horizontal pressure gradient and bore turbulence, which together represent the hydrodynamic forcing. The model was validated against two data sets of sheet flow layer thickness collected in oscillatory flow tunnels and one data set collected in the swash zone of a prototype-scale laboratory experiment. In the oscillatory flow tunnel data sets, sheet flow is mostly generated by shear stress, with pressure gradients providing an important secondary forcing around flow reversal. In the swash zone, pressure gradients and shear stresses alone are not sufficient to generate the large sheet flow layer thickness observed at the initial stages of uprush. Bore turbulence is most likely the dominant generation mechanism for this intense sheet flow.

1. Introduction

Sediment transport in the near-shore consists of two parts: suspended transport and near-bed transport. In the swash zone, near-bed sediment transport is the dominant transport mode during the backwash, and is also important during the uprush [Horn and Mason, 1994; J. A. Puleo et al., Sediment transport partitioning in the swash zone of a large-scale laboratory beach, submitted to *Coastal Engineering*, 2014]. The importance of near-bed sediment transport in the swash zone is in part due to the strong hydrodynamic forcing, which generates sheet flow throughout a large portion of the swash cycle [Lanckriet et al., 2014], and in part because the small water depths constrain the capacity for suspended sediment transport, despite high observed suspended sediment concentrations [Butt and Russell, 1999; Puleo et al., 2000; Masselink et al., 2005].

Experimental studies to investigate sheet flow have been conducted primarily in oscillatory flow tunnels [Horikawa et al., 1982; Ribberink and Al-Salem, 1995; Dibajnia and Watanabe, 1998; Dohmen-Janssen et al., 2001; Ahmed and Sato, 2003; O'Donoghue and Wright, 2004a, 2004b; van der A et al., 2010; Ruessink et al., 2011; Dong et al., 2013], supplemented by wave flume studies [Dohmen-Janssen and Hanes, 2002, 2005; Chassagneux and Hurther, 2014]. A main outcome was the development of empirical formulas for the net sheet flow sediment transport aimed toward use in large-scale morphodynamic models [Drake and Calantoni, 2001; Hoefel and Elgar, 2003; Watanabe and Sato, 2004; Camenen and Larson, 2006; da Silva et al., 2006; Nielsen, 2006; Gonzalez-Rodriguez and Madsen, 2007; van der A et al., 2010, 2013]. Formulas for other parameters such as the maximum sheet flow layer thickness, δ_s , and the maximum erosion depth, δ_e , were also proposed.

Many past experiments simplified the sheet flow process by using repeatable wave forcing (e.g., sinusoidal, skewed or asymmetric waves) and excluding breaking wave-generated turbulence. These conditions form a realistic representation of hydrodynamic conditions under shoaling waves and in the outer surf zone, where breaking wave-generated turbulence has limited potential to mobilize near-bed sediment. In contrast, the near-bed layer in the inner surf and swash zones is directly affected by bore-generated turbulence [Puleo et al., 2000; Butt et al., 2004; Jackson et al., 2004; Aagaard and Hughes, 2006; Lanckriet and Puleo, 2013]. The impact of breaking wave-generated turbulence on the sheet flow layer has only recently been investigated

[Chassagneux and Hurther, 2014]. In addition to bore turbulence, there are a number of other swash-zone processes that affect the sheet flow layer, including pressure gradients, which exert a mobilizing force on sediment grains [Puleo et al., 2003, 2007; Othman et al., 2014], and groundwater infiltration and exfiltration, which alters the boundary layer and the effective stresses on the bed [Turner and Masselink, 1998; Butt et al., 2001; Karambas, 2003]. At the swash tip, flow convergence and an underdeveloped boundary layer generate increased friction and shear stresses [Barnes and Baldock, 2010; Baldock et al., 2014]. In addition, swash motions on a dissipative beach are a mixture of wind waves that generate oscillatory sheet flow and infra-gravity motions that generate long-duration sheet flow events that resemble stationary, unidirectional sheet flow [Lanckriet et al., 2014]. These additional phenomena cannot be incorporated readily in existing empirical formulas for sheet flow. Alternatively, analytical models can improve the understanding of the mechanics of sheet flow, even if their predictions are not necessarily as accurate as empirical models.

This paper presents a new semianalytical model for the time-dependent sheet flow layer thickness $\delta_s(t)$ under generalized forcing conditions, including conditions that occur in the swash zone. The sheet flow layer thickness is chosen as the modeled parameter because measured time series of $\delta_s(t)$ are available under realistic swash-zone conditions that can be used to validate the model. In contrast, the near-bed sediment transport rate is a more important parameter for practical applications but measured time series of the sheet flow transport rate are not yet available in the swash zone.

Two-phase numerical models that resolve the granular dynamics and sediment-fluid interactions have led to an improved understanding of sheet flow [Hsu et al., 2004; Calantoni and Puleo, 2006; Amoudry et al., 2008; Bakhtyar et al., 2009, 2010; Chen et al., 2011]. However, the mechanics of sheet flow are not yet fully understood, especially in complex natural environments such as the swash zone. The model proposed here uses a different approach than most two-phase models and divides the flow into two layers: the sheet flow layer and the remainder of the water column, where sediment concentrations are dilute. The model regards the sheet flow layer as a “bulk” entity and assumes that $\delta_s(t)$ can be predicted based on quantities at the top and bottom of the sheet flow layer. This approach avoids the need to resolve the complex intergranular interactions inside the sheet flow layer, at the cost of a certain degree of approximation. The model predicts the shear stress from the flow above the sheet flow layer using the momentum integral method [Fredsoe, 1984; Briganti et al., 2011]. An alternative two-layer model has been proposed [Malarkey et al., 2003, 2009] that uses an empirically based parameterization of the sheet flow layer combined with a $k - \epsilon$ turbulence closure model in the upper water column.

The main objective of the new model is to show the relative importance of different forcing mechanisms for sheet flow in the swash zone. For example, onshore-directed pressure gradients, bore-generated turbulence and underdeveloped boundary layers all occur simultaneously at the time of bore arrival, resulting in intense sheet flow [Lanckriet et al., 2013]. The importance of the three phenomena is difficult to separate because an empirical analysis of one of the mechanisms may implicitly include the effect of the other two mechanisms [Puleo et al., 2003]. An analytical model that is based on the different forces can provide new insight about the leading cause of intense sheet flow upon bore arrival.

Furthermore, near-bed sediment may be mobilized by strong pressure gradients as plug flow [Sleath, 1999; Foster et al., 2006; Frank et al., 2014; Othman et al., 2014]. In natural environments, pressure gradients occur along with shear stress meaning that near-bed transport may be a combination of sheet flow and plug flow. The effect of pressure gradients is implicitly accounted for in existing empirical formulas, and an analytical derivation of the inception of motion for plug flow has been developed [Sleath, 1999]. However, an analytical framework that unifies sheet flow and plug flow has so far only been suggested [Foster et al., 2006].

An existing analytical formula for the sheet flow layer thickness under stationary flow is [Wilson, 1987]:

$$\frac{\delta_s}{d_{50}} = \Lambda \theta, \tag{1}$$

where d_{50} is the median grain diameter, Λ is a dimensionless coefficient and θ is the Shields number:

$$\theta = \frac{\tau}{g(\rho_s - \rho)d_{50}}, \tag{2}$$

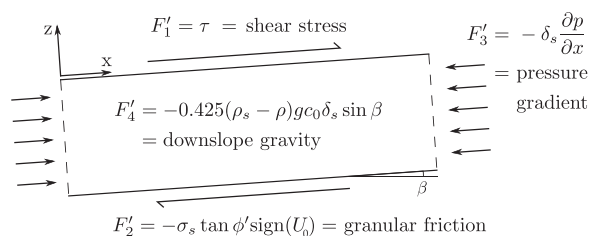


Figure 1. Force balance upon the sheet flow layer

with τ the shear stress near the bed, ρ is the water density, ρ_s is the sediment density, and g is gravitational acceleration. *Wilson* [1987] derived (1) analytically from a force balance between the shear stress and the granular friction (based on a dynamic Coulomb yield criterion that was originally proposed by *Bagnold* [1956, 1966]) and estimated $\Lambda \approx 10$. Good agreement between (1) and measurements of (quasi-

stationary sheet flow has been observed [*Sumer et al.*, 1996; *Langkriet et al.*, 2014]. Equation (1) has also been used to predict the quasi-steady and maximum sheet flow layer thickness under oscillatory flow [*Dohmen-Janssen et al.*, 2001; *Malarkey et al.*, 2003; *Dong et al.*, 2013].

The remainder of this paper is organized as follows. The semianalytical model is described in section two. Data sets from three different studies (two in an oscillatory flow tunnel and one in the swash zone) were used to validate the model and are described in section three. Results of the model-data comparison are presented in section four. Section five discusses the development, performance and implications of the model, and section six provides conclusions.

2. Model Development

2.1. Sheet Flow Layer Thickness

Throughout the vertical extent of the water column, the total shear stress can be divided into a fluid and a granular shear stress component [*Bagnold*, 1956]. The total shear stress is equal to the granular shear stress (fluid shear stress equal to zero) at the top of the nonmoving bed (the bottom of the sheet flow layer). In the dilute region above the sheet flow layer, grain-grain interactions are rare and the granular shear stress is negligible. Following results from two-phase numerical models [*Hsu et al.*, 2004; *Amoudry et al.*, 2008], the proposed model assumes that the sediment shear stress is negligible at the elevation where the sediment volumetric concentration equals 0.08, which is defined as the top of the sheet flow layer [see also *Dohmen-Janssen and Hanes*, 2002, 2005; *Malarkey et al.*, 2003, 2009; *O'Donoghue and Wright*, 2004a, among others]. The total shear stress is thus transferred from the fluid phase to the sediment phase within the sheet flow layer through sediment-fluid interactions. The proposed model does not resolve these interactions or the shear stress transfer, but instead regards the sheet flow layer as a “bulk entity” and considers only forces at the top and bottom of the layer.

The starting point for the model development is the analytical formula for sheet flow layer thickness of *Wilson* [1987] (equation (1)). The equation was derived from a force balance between the fluid shear stress at the top of the sheet flow layer and the granular friction at the bottom of the layer, using a dynamic Coulomb yield criterion that was originally proposed by *Bagnold* [1956, 1966]. The derivation is extended here by considering a balance of four forces acting upon a sheet flow layer with thickness $\delta_s(t)$, located on a bed with slope β , and over a unit planform area A (Figure 1). All forces act in the bed-parallel direction and are defined positive in the direction of wave propagation and runup (uphill).

The four forces (per unit area) are:

1. Shear stress at the top of the sheet flow layer τ :

$$F'_1 = F_1/A = \tau \quad (3)$$

2. Dynamic friction between the moving sheet flow layer and the nonmoving bed:

$$F'_2 = F_2/A = -\sigma_s \tan \phi' \text{sign}(U_0) \quad (4)$$

where σ_s is the normal force between the sheet flow layer and the nonmoving bed, U_0 is the bed-parallel free-stream velocity and ϕ' is the dynamic friction angle. The value $\tan \phi' = 0.32$ was adopted [*Wilson*, 1987]. σ_s was calculated as [*Wilson*, 1987]:

$$\sigma_s = \cos \beta (\rho_s - \rho) g \int_0^{\delta_s} c(z) dz \quad (5)$$

The sediment concentration profile in the sheet flow layer $c(z)$ was assumed to follow a curve proposed by O'Donoghue and Wright [2004a]:

$$c(z) = c_0 \frac{1}{1 + \left(\frac{z}{\delta_s}\right)^\alpha \frac{c_0 - c_t}{c_t}} \tag{6}$$

where $c_0 = 0.625$ is the concentration at the bottom of the sheet flow layer [Wilson, 1987], $c_t = 0.08$ is the concentration at the top of the sheet flow layer, and α is a shape factor. Lanckriet et al. [2014] found good agreement of (6) with field measurements in the swash zone using $\alpha = 1.73$. Integration of (5) then yields:

$$\sigma_s = 0.425(\rho_s - \rho)g c_0 \delta_s \cos \beta \tag{7}$$

3. Pressure gradient force:

$$F'_3 = F_3/A = -\delta_s \frac{\partial p}{\partial x} \tag{8}$$

where p indicates pressure.

4. Downslope gravity:

$$\begin{aligned} F'_4 = F_4/A &= -\sin \beta \int_0^{\delta_s} (\rho_s - \rho)g c(z) dz \\ &= -0.425(\rho_s - \rho)g c_0 \delta_s \sin \beta \end{aligned} \tag{9}$$

A force balance between the four forces yields:

$$\frac{\tau}{(\rho_s - \rho)g d_{50}} = \frac{\delta_s}{d_{50}} \left\{ \frac{\partial p}{\partial x} + 0.425 c_0 [\tan \phi' \cos \beta \text{sign}(U_0) + \sin \beta] \right\} \tag{10}$$

or

$$Y = \frac{\theta}{0.425 c_0 [\tan \phi' \cos \beta \text{sign}(U_0) + \sin \beta] - S} \tag{11}$$

with $Y = \delta_s(t)/d_{50}$ the dimensionless sheet flow layer thickness and $S = -\frac{\partial p}{(\rho_s - \rho)g}$ the Sleath number. In the case of stationary, unidirectional flow ($S = 0$) over a horizontal bottom ($\beta = 0$), (11) reduces to Wilson's [1987] formula (equation (1)) with $\Lambda = 11.8$ [Lanckriet et al., 2014]. For the case of no external pressure gradient ($S = 0$), downhill flow ($U_0 < 0$) and the bed slope equal to the friction angle ($\phi' = \beta$), δ_s diverges to infinity, representing slope failure. For pressure gradient values commonly observed in the nearshore such as $\tan \beta = 0.05$ (a 1 : 20 beach slope), $U_0 > 0$ (uprush) and $S = 0.10$, δ_s diverges to infinity as well. This divergence does not occur in reality because pressure gradient peaks in the nearshore are short-lived and the sheet flow layer thickness does not respond instantaneously to external forcing. Instead, the sheet flow layer has a finite response time and does not reach its (large) thickness value in the short time span that the pressure gradient occurs.

The model is therefore extended to include the finite response time necessary to displace sediment grains and alter the sheet flow layer thickness. This lag is likely related to the settling velocity w , and we propose on dimensional grounds:

$$C_1 = (\rho_s - \rho)w \text{sign}(U_0) \frac{d\delta_s}{dt} = \sum_{i=1}^4 F'_i \tag{12}$$

where C_1 is a dimensionless parameter. Inserting the force terms leads to:

$$\begin{aligned} C_1 = \frac{w}{g} \frac{dY}{dt} &= -Y \left(0.425 c_0 [C_2 \tan \phi' \cos \beta + \sin \beta \text{sign}(U_0)] - S \text{sign}(U_0) \right) \\ &\quad + \theta \text{sign}(U_0) \end{aligned} \tag{13}$$

A second dimensionless parameter, C_2 , is introduced in (13) to account for uncertainty in the dynamic friction angle ϕ' .

Large sheet flow layer thicknesses were observed upon bore arrival in the swash zone that may have been caused by bore-generated turbulence. Bore turbulence is not a force and cannot be incorporated directly in the force balance on the right-hand side of (13). An estimate of the bore turbulence effect is defined by D/h , the breaking wave energy dissipation per unit volume [Battjes and Janssen, 1978]

$$\frac{D}{h} \sim \frac{1}{4} \rho g \frac{H^3}{h^2 T}, \tag{14}$$

where T is the wave period, H is the bore height and h is the average water depth. The potential energy, PE , of the grains mobilized in the sheet flow layer is proportional to

$$PE \sim (\rho_s - \rho) g \frac{\delta_s}{2}, \tag{15}$$

Assuming that the change in potential energy of the sheet flow layer is proportional to the wave energy dissipation yields:

$$\frac{1}{2} (\rho_s - \rho) g \frac{d\delta_s}{dt} \sim \frac{1}{4} \rho g \frac{H^3}{h^2 T} \tag{16}$$

or

$$\frac{w dY}{g dt} \sim \frac{1}{2} \frac{w}{g} \frac{\rho}{\rho_s - \rho} \frac{H^3}{h^2 d_{50} T} = \frac{1}{2} B, \tag{17}$$

where B is the dimensionless bore term. Equations (13) and (17) are combined by adding the bore turbulence term to the right-hand side of (13), yielding:

$$C_1 = \frac{w dY}{g dt} = -\gamma \left(0.425 c_0 \left[C_2 \tan \phi' \cos \beta + \sin \beta \operatorname{sign}(U_0) \right] - S \operatorname{sign}(U_0) \right) + \theta \operatorname{sign}(U_0) + C_3 B, \tag{18}$$

where C_3 is a dimensionless parameter that absorbs the factor of 1/2 in equation (17).

2.2. Shear Stress

The time-dependent shear stress at the top of the sheet flow layer is calculated following the boundary layer integral method [Fredsoe, 1984; Fredsoe and Deigaard, 1992] that was applied to the swash zone by Briganti et al. [2011] (a different formulation of the boundary layer integral method was applied to the swash zone by Barnes and Baldock [2010]). The formulation by Fredsoe and Deigaard [1992] is stated in terms of a dimensionless parameter

$$Z(t) = \frac{U_0(t)}{U_* (t)} k, \tag{19}$$

where $U_* = \sqrt{\tau/\rho} \operatorname{sign}(U_0)$ is the friction velocity, and $k = 0.41$ is the von Karman constant. The boundary layer integral method assumes a logarithmic velocity profile in the boundary layer:

$$u(z, t) = \frac{U_*}{k} \ln \left(\frac{z}{z_0} \right), \tag{20}$$

where $z_0 = K_n/30$, with K_n the bed roughness. Evaluating (20) at $z = \delta_b$, the boundary layer thickness, yields $Z = \ln \left(\frac{\delta_b + z_0}{z_0} \right)$. The horizontal momentum equation, integrated vertically across the boundary layer thickness, can then be expressed in terms of Z :

$$\frac{dZ}{dt} = \left(\frac{k^2 U_0}{z_0} - Z(e^Z - Z - 1) \frac{1}{U_0} \frac{dU_0}{dt} - \frac{e^Z - 1}{z_0} \frac{dz_0}{dt} \right) / (e^Z (Z - 1) + 1). \tag{21}$$

The term $\frac{e^Z - 1}{z_0} \frac{dz_0}{dt}$ in (21) reflects the time-varying bed roughness and was not included in the original derivation of Fredsoe [1984].

Under mobile-bed conditions, the bed roughness K_n includes contributions from the grain diameter K_{gs} and the sheet flow layer thickness K_{st} [Ribberink, 1998; Da Silva et al., 2006]:

$$K_n = K_{ss} + K_{st} \tag{22}$$

with $K_{ss} = 2.5 d_{50}$. Since the sheet flow layer thickness is determined directly in the model presented here, the mobile-bed contribution is expressed as $K_{st} = 0.5 \delta_s$ following *Wilson* [1989].

In summary, equations (18) and (21) form a set of two coupled ordinary differential equations (ODEs) for the dimensionless sheet flow layer thickness Y and dimensionless boundary layer constant Z . The shear stress $\tau = \rho |U_*| U_*$ which is one of the forcing terms in (18), is obtained from the solution of (21) and (19). The sheet flow layer thickness $\delta_s(t)$ is solved in (18) and determines the bed roughness in (21) through (22). The two ODEs were solved using a variable-order numerical method (the ode15s solver in MATLAB [*Shampine and Reichelt*, 1997]) given an input time series of $U_0(t)$, $\frac{\partial p(t)}{\partial x}$ and $B(t)$, which represent hydrodynamic forcing.

The model contains three dimensionless parameters C_1 , C_2 , and C_3 that represent the lag effect of the sheet flow layer, uncertainties in the frictional resistance at the bottom of the sheet flow layer, and the effect of bore-generated turbulence, respectively. The dimensionless parameters were calibrated using a procedure that is described in the Appendix A which optimizes both the Pearson correlation coefficient r^2 (equation (A1)) and the Root Mean Square Error (RMSE, equation (A2)). The model code is freely available upon request from the authors.

3. Measurement Data Sets

The model was validated using measurements of $\delta_s(t)$ from three laboratory studies. The three data sets were combined into two data groups depending on the type of forcing:

1. An oscillatory flow tunnel data group that consists of two data sets collected by *O'Donoghue and Wright* [2004a] and *Ruessink et al.* [2011].
2. A swash zone data group that consists of one data set collected by *Puleo et al.* (submitted manuscript).

For each sediment used in the experiments, the settling velocity, w , of the median grain size d_{50} was calculated as:

$$w = \sqrt{\frac{4(\rho_s - \rho)gd_{50}}{3\rho C_D}} \tag{23}$$

with $C_D = 1.4 + 36/\text{Re}$ the particle drag coefficient [*Fredsøe and Deigaard*, 1992] and $\text{Re} = \frac{wd_{50}}{\nu}$ the particle Reynolds number.

3.1. Oscillatory Flow Tunnel Data Group

A first data set of $\delta_s(t)$ was collected in the Aberdeen Oscillatory Flow Tunnel (AOFT), for four different flow conditions (two sinusoidal flows and two second-order Stokes skewed flows) and seven different sediment sizes (well-sorted fine, medium and coarse sand, and four sand mixtures) [*O'Donoghue and Wright*, 2004a]. Sediment concentrations in the sheet flow layer were measured using several Conductivity Concentration Meters (CCMs) [*Ribberink and Al-Salem*, 1995]. The CCMs are single-point probes that measure sediment concentration using electrical conductivity as a proxy. Experiments were repeated several times with the CCMs positioned at different elevations to capture the time-dependent sediment concentration profile, which was then used to calculate $\delta_s(t)$. Data were only available for the skewed flow cases. Only the time series with well-sorted medium and coarse sand were chosen to calibrate the model since the fine sand case was likely dominated by suspended sediment (see section 5.1).

A second data set was collected in the Large Oscillatory Water Tunnel (LOWT) at Deltares, the Netherlands as part of the TRANSKEW project [*Ruessink et al.*, 2011]. The sheet flow layer thickness was derived from CCM measurements in a similar manner as *O'Donoghue and Wright* [2004a] for five different flow conditions: two asymmetric flows, the same two asymmetric flows superimposed on a net countercurrent and a mixed skewed-asymmetric flow. A well-sorted medium sand was used for all cases. The two data sets were aggregated into one oscillatory flow tunnel data group, comprising nine cases with different flow conditions and three different sediment sizes (Table 1). In the test section of an oscillatory flow tunnel, $\frac{\partial u}{\partial x} = 0$. The pressure gradient was therefore derived from the velocity time series as

Table 1. Summary of Oscillatory Flow Tunnel Data Group

Case	Waveform Shape	d_{50} (mm)	w (m/s)	T (s)
<i>O'Donoghue and Wright [2004a]</i>				
MA5010	Skewed	0.28	0.034	5.0
MA7515	Skewed	0.28	0.034	7.5
CA5010	Skewed	0.51	0.067	5.0
CA7515	Skewed	0.51	0.067	7.5
<i>Ruessink et al. [2011]</i>				
A1	Asymmetric	0.20	0.021	7
A3	Asymmetric	0.20	0.021	7
B2	Asymmetric with countercurrent	0.20	0.021	7
B4	Asymmetric with countercurrent	0.20	0.021	7
C1	Skewed-asymmetric	0.20	0.021	7

$$\frac{\partial p}{\partial x} = -\rho \frac{\partial U_0}{\partial t}. \quad (24)$$

3.2. Swash Zone Data Group

Sheet flow in the swash zone was studied by the authors during the BARDEX II experiment (*Puleo et al.*, submitted manuscript). A near-prototype scale barrier island composed of medium sand ($d_{50} = 0.43$ mm; $w = 0.056$ m/s) was constructed in the Deltaflume at Deltares, the Netherlands. Sheet flow sediment concentrations were measured in the swash zone of the barrier island using the Conductivity Concentration Profiler (CCP). The CCP measures sediment concentration based on electrical conductivity in a manner similar to the CCM but samples the entire concentration profile simultaneously over a vertical range of 29 mm [*Lanckriet et al.*, 2013]. The profiling capability avoids the need for multiple repetitions of a given set of regular forcing conditions and makes it possible to study sheet flow under irregular (nonrepeatable) wave forcing. The CCP accurately resolves sheet flow with $\delta_s(t) > 5$ mm, meaning that instances with $\delta_s(t) \leq 5$ mm were not included in the measurement time series.

Figure 2 displays an overview of the experiment setup in a flume coordinate system (x' , z') where the cross-shore coordinate $x' = 0$ m at the wave maker (in its neutral position) and the vertical coordinate $z' = 0$ m at the flume bottom. The CCP was placed at $x' = 89.6$ m (Figure 2, magenta), approximately 2.6 m landward of the shoreline at the start of the wave run. An electromagnetic current meter (EMCM) was located at the same cross-shore location, positioned 0.06 m above the bed and measured cross-shore and along-shore

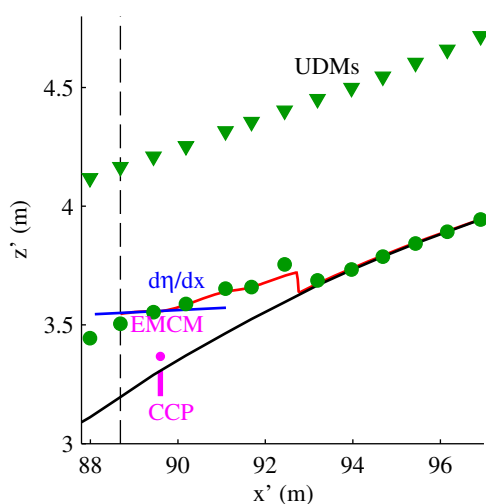


Figure 2. Experiment setup of sheet flow measurements in the swash zone during BARDEX II. Green circles: free surface/bottom level measured by UDM array. Green triangles: location of UDM array. Black solid curve: beach profile derived from UDM array measurements. Red curve: swash free surface modeled by FUNwave model. Black dashed line: offshore boundary of the FUNwave model.

horizontal velocities. A cross-shore array of ultrasonic distance meters (UDMs) with a 0.75 m spacing was deployed throughout the inner surf and swash zones (Figure 2, green triangles) and measured the free surface elevation of the swash lens during swash events, and the beach profile elevation in between swash events when the bed was exposed (Figure 2, green circles).

This paper focuses on a $\delta_s(t)$ time series collected during a 15 min wave run of test series A6 of the BARDEX II experiment. Conditions for series A6 consisted of a water depth of 3 m both in front of the barrier (the 'sea') and behind it (the 'lagoon') so that there was no strong groundwater flow through the barrier that may affect sediment transport. The wave forcing during this test series was composed of irregular waves with a JONSWAP spectrum with peak enhancement factor 3.3, peak period $T_p = 12$ s, and significant wave height of 0.6 m. The sheet flow layer was not captured by the CCP for the entire wave run due to fluctuations in the swash zone bed level [*Puleo et al.*, 2014a]. Therefore, an excerpt of the wave run with a

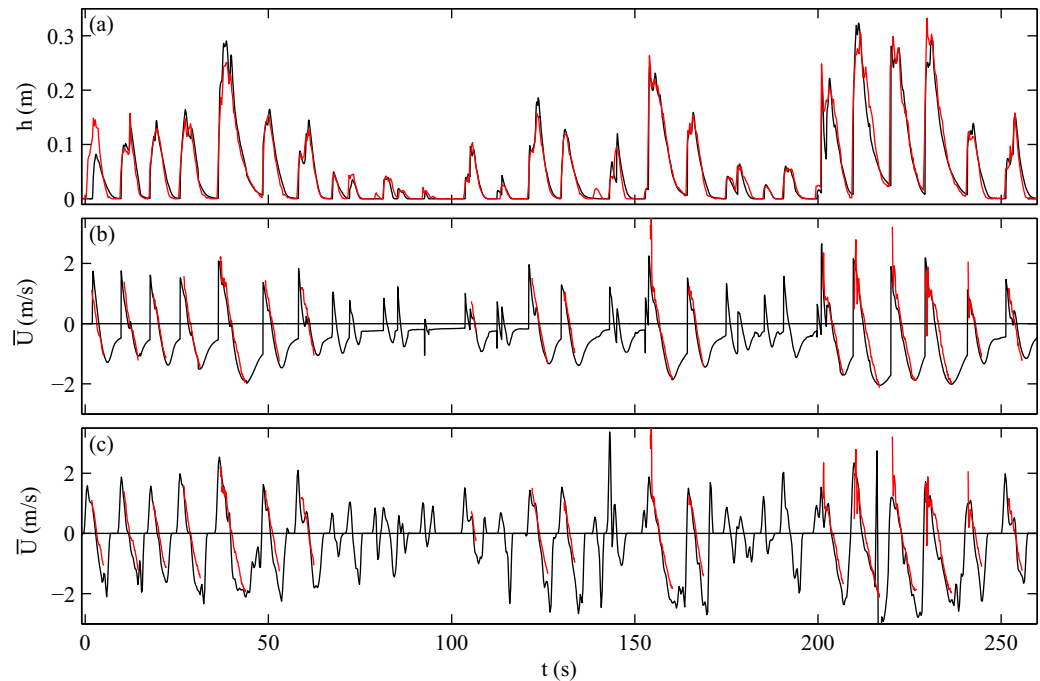


Figure 3. (a) Comparison of measurements of water depth (red) and FUNwave model result (black). (b) Comparison of measurements of cross-shore velocity from the EMCM (red) and FUNwave model result (black). (c) Comparison of measurements of cross-shore velocity from the EMCM (red) and velocity estimate using volume continuity method (black).

duration of 261 s (containing 29 swash events) during which the sheet flow layer was captured continuously by the CCP, was retained to validate the sheet flow layer model.

3.2.1. Reconstructing Velocity Time Series

The sheet flow layer model requires an uninterrupted velocity time series as a model input. In the swash zone, in situ velocimeters do not record a velocity signal when the water level is below the velocimeter elevation, leaving gaps in the velocity record [Puleo *et al.*, 2014b]. The cross-shore velocity time series for these data gaps was reconstructed using two methods: the volume continuity method and a nonlinear shallow water equation solver. Water depth and velocity estimates from both methods are compared to in situ measurements in Figure 3.

First, the depth-averaged velocity \bar{U} was estimated using the UDM array measurements and the volume continuity method [Baldoock and Holmes, 1997; Houser and Barrett, 2009; Blenkinsopp *et al.*, 2010]. Flow velocities measured by the EMCM and estimated by the volume continuity method are compared in Figure 3c. The volume continuity method estimates depth-averaged velocity by dividing cross-shore volume flux by local water depth. Spurious velocity estimates are occasionally produced when the volume flux and water depth are both small at the end of the backwash phase (Figure 3c, $t = 15$ s, 162 s, 238 s). The RMSE between EMCM measurements and volume continuity method estimates of the cross-shore velocity was 0.604 m/s and r^2 was 0.78.

A second estimate of the depth-averaged velocity was produced using a numerical model in order to eliminate the spurious velocity estimates. FUNwave, a Boussinesq wave model [Shi *et al.*, 2012], was used as a shock-capturing nonlinear shallow water equation solver by deactivating the Boussinesq terms. FUNwave was run in one-dimensional mode over the beach bathymetry measured by the UDM array, with a cross-shore grid spacing of 0.025 m. The offshore boundary of the model was located 0.91 m seaward of the CCP location (Figure 2, dashed vertical line). At the offshore boundary, the model was forced by specifying the depth-averaged velocity and water depth h estimated from the UDM array and the volume continuity method, ensuring that the swash lens volume in the FUNwave model domain is equal to the volume measured by the UDM array at each time step. A constant friction factor of $f = 0.009$ was used. The friction and inertia terms in FUNwave naturally dissipate spurious velocities in the \bar{U} forcing at the seaward boundary of

the model, creating a depth-averaged velocity time series at the CCP location that was similar to the time series estimated by the volume continuity method but without spurious velocity estimates. FUNwave results are compared against measured time series of local water depth (measured by the UDM array) and cross-shore flow velocity (measured by the EMCM) in Figures 3a and 3b, respectively. Agreement between the measured and modeled water depth (RMSE = 0.019 m; $r^2 = 0.92$) and velocity (RMSE = 0.4 m/s; $r^2 = 0.88$) are both good. Visual inspection of the velocity time series (see also Figure 5b) indicate that two main sources of error were (1) differences in the flow phase which were likely due to the EMCM and UDM measurements not being perfectly synchronized in time, and (2) spurious velocity measurements at the start of the uprush cycle (e.g., at $t = 154$ s) when the EMCM had just become submerged by the swash lens. The FUNwave model provided an accurate and continuous estimate of the cross-shore velocity time series over the volume continuity method and was thus used as the input for the sheet flow layer model. The free-stream velocity U_0 was calculated from the depth-averaged velocity \bar{U} by accounting for the reduced velocity in the boundary layer, using the equations in *Briganti et al.* [2011, Appendix A] (adopted from *Clarke et al.* [2004]).

Unlike for oscillatory flow tunnel experiments, $\frac{\partial U_0}{\partial t}$ is not a robust proxy for the pressure gradient in the swash zone because advected acceleration terms are important [*Baldock and Hughes, 2006; Puleo et al., 2007; Othman et al., 2014*]. Instead, the pressure gradient was calculated from the free surface elevation η [*Othman et al., 2014*]:

$$\frac{\partial p}{\partial x} = \rho g \frac{\partial \eta}{\partial x}. \quad (25)$$

$\frac{\partial \eta}{\partial x}$ was determined by fitting a straight line through FUNwave output of $\eta(x, t)$ at 9 grid points around the $\delta_s(t)$ measurement location (Figure 2, blue line). The bottom slope β , needed for the sheet flow model, was calculated from the bathymetry measurements obtained from the UDM array (Figure 2, black curve). For the time series presented here, $\tan \beta = 0.114$ (gradient 1:9), a steep slope.

3.2.2. Bore Turbulence Term

The nondimensional bore turbulence term B (equation (17)) was calculated as follows. Bore events were identified as increases of 0.04 m or more in the local water depth $h(t)$ over a duration of 2 s or less based on visual observations made by the authors during the experiment and an examination of the measured water level time series. Water depths h_1 and h_2 were then defined as the minimum and maximum measured depth during the 2 s window. The bore height H and bore water depth h were then calculated as $H = h_2 - h_1$ and $h = \frac{h_2 + h_1}{2}$. The time scale T during which the bore affected the sediment bed is difficult to determine. The bore effect on the near-bed layer is assumed to be largest at the first stage of bore arrival when the water depth is small and then decrease as the growing water depth increases the distance between the surface bore and the sheet flow layer. Observations of the sheet flow layer during the first moments of the uprush (e.g., Figure 5h, $t = 209$ s, 220 s, 229 s) suggest that a large layer of sediment (up to 0.01 m) was mobilized rapidly within the time span of one sampling interval of the CCP sensor (0.125 s). Since the evolution of bore turbulence could not be studied at a higher temporal resolution, T was set equal to the CCP sampling frequency ($T = 0.125$ s) and the bore term B was set to its calculated value for the duration of 0.125 s and to zero when no bore event occurred.

4. Results

4.1. Oscillatory Flow Tunnel Data Group

The model was run for 15 wave cycles to allow for the spin-up of the sheet flow layer. Model results from the final wave cycle were retained for further analysis. Results are displayed in Figure 4. Model skill statistics are summarized in Table 2. The sheet flow layer thickness predicted by the model (black curves, plots 51–59) shows good agreement with the measurements (red curves). Tests CA5010 and CA7515 were run over a coarse sand bed ($d_{50} = 0.51$ mm) but experienced the same hydrodynamic forcing as runs MA5010 and MA7515, respectively, which were conducted over medium sand ($d_{50} = 0.28$ mm). The main effect of the grain size on the measured $\delta_s(t)$ (red curve, plots 56–59) is that the medium sand (with a smaller fall velocity w) exhibits a faster response to the hydrodynamic forcing, resulting in a more peaked $\delta_s(t)$ time series, especially during the crest of the simulated wave cycle ($U_0 > 0$). This observation motivated the formulation of

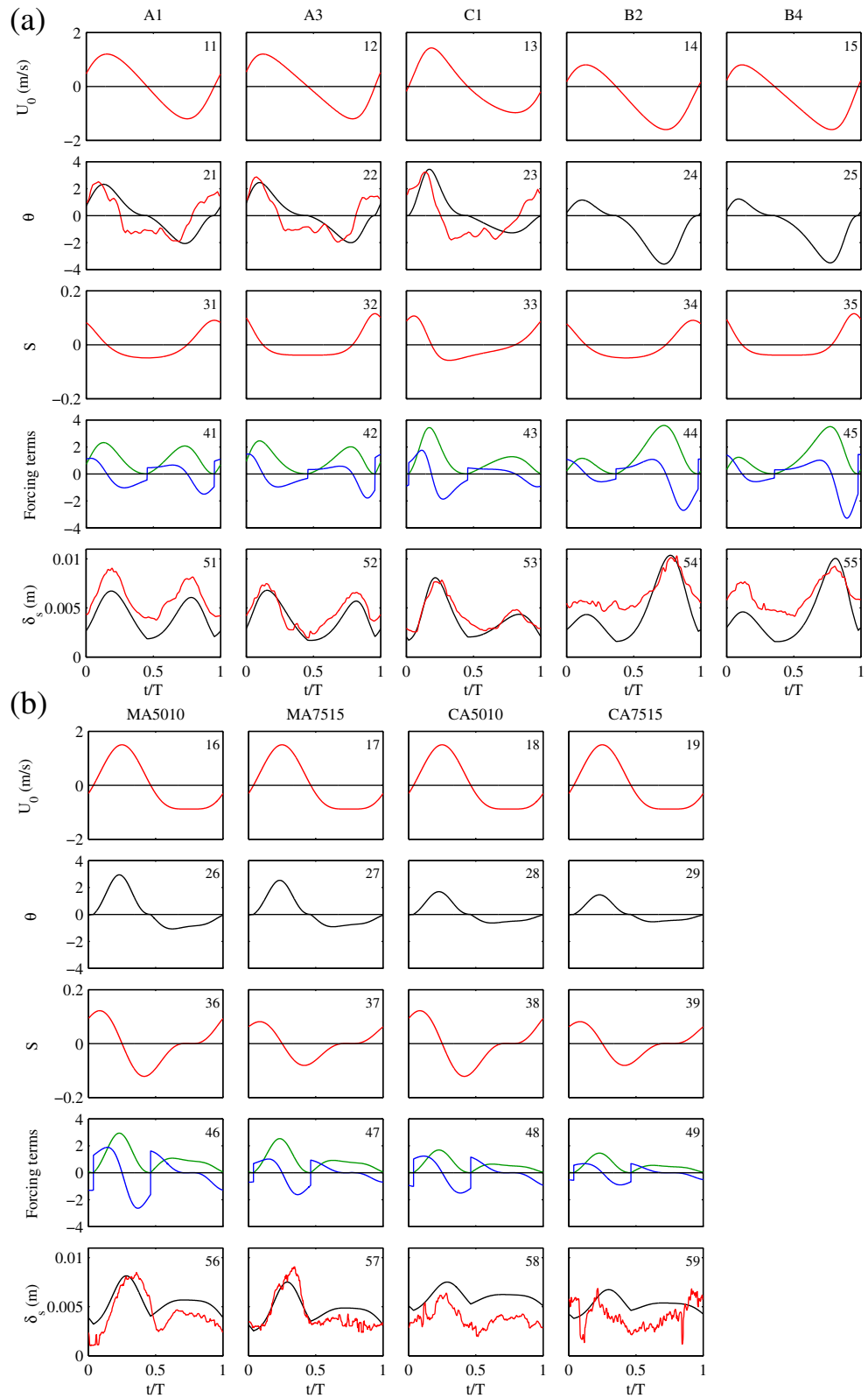


Figure 4. Model results (black curves) and measurements (red curves) for the oscillatory flow tunnel data set. Top row (plots 11–19): Free stream velocity. Second row (plots 21–29): Shields number. Third row (plots 31–39): *Sleath* number. Fourth row (plots 41–49): Mobilizing force terms. Green curve is $\theta \text{ sign}(U_0)$; blue curve is $YS \text{ sign}(U_0)$. Fifth row (plots 51–59): Sheet flow layer thickness.

Table 2. Model Skill Statistics and Calibration Coefficients for the Sheet Flow Layer Thickness Model^a

	RMSE (mm)	r^2	R^2	BSS	C_1	C_2	C_3
Oscillatory flow tunnel data set	1.70	0.34	0.15	0.62	41.65	0.57	/
Swash Zone Data Set							
Complete time series	4.15	0.33	-0.95	0.32	49.56	1.71	317.36
Excluding swash events < 0.07 m	3.71	0.38	-0.45	0.38	49.56	1.71	317.36

^aModel skill statistics described in the Appendix A.

the sheet flow layer lag term using w (equation (12)) so that the model replicates the faster response time for smaller w (black curve, plots 56–69).

Tests A1, A3, and C1 also included measurements of the shear stress. The modeled shear stress (represented by the nondimensional Shields number) also shows good agreement with the measurements (plots 21–23), particularly with respect to the magnitude of the peak positive and negative shear stress. This demonstrates that the boundary layer integral method (equation (21)), and the bottom roughness formulation (equation (22)), provided a realistic description of the shear stress.

Since the bottom slope β and the bore-generated turbulence term B are both zero in the oscillatory flow tunnel experiments, equation (18) is simplified to a balance between two mobilizing forces: the pressure gradient [$Y \text{ sign}(U_0)$] and the shear stress [$\theta \text{ sign}(U_0)$], and the resisting force $-0.425 Y c_0 [C_2 \tan \phi' \cos \beta]$. The mobilizing forces are dominated by the shear stress (green curve, plots 41–49), even though the pressure gradient term provides an important contribution as well. The pressure gradient is dominant only during the initial moments after flow reversal, particularly for waveforms with a strong skewness (e.g., plot 46).

4.2. Swash Zone Data Group

A time series excerpt of the model results from the swash zone data group is displayed in Figure 5. Model results for the full swash zone time series are displayed in supporting information Figure 1 (available with the online version of this paper). Good agreement is again observed between measured and modeled sheet flow layer thickness (Figure 5g). The model discrepancy was larger during small swash events (maximum water depth less than 0.07 m, e.g., at $67s \leq t \leq 100s$, Figure 3). These larger discrepancies likely occurred because errors in the FUNwave model (section 3.2.1) that provided the hydrodynamic input for the sheet flow layer model had a relatively larger impact during these smaller events. Model skill statistics (Table 2) are provided for both the entire time series and for the time series excluding sheet flow during swash events with a maximum water depth less than 0.07 m, which are deemed to be not well resolved by the FUNwave model [20% of $\delta_s(t)$ measurements].

The sheet flow model predicted large sheet flow layer thicknesses upon bore arrival (e.g., $t = 210s, 220s, 230s$). During these times, no values of $\delta_s(t)$ were available because the sheet flow layer was not entirely captured within the vertical profiling range of the CCP. However, measurements of the sediment concentration profile (Figure 5h) from which $\delta_s(t)$ was derived, indicate that the sheet flow layer thickness was at times larger than the CCP profiling range (29 mm) during these instances.

The pressure gradient (represented by the Sleath number; Figure 5d) was mostly offshore-directed (in agreement with field measurements [Baldock and Hughes, 2006]), but was interrupted by strong onshore-directed pressure gradient peaks upon bore arrival (e.g., at $t = 220s$). Forcing terms are summarized in Figures 5e and 5f. Two additional mobilizing mechanisms affect $\delta_s(t)$ compared to the oscillatory flow tunnel experiments: the downslope gravity (Figure 5e, magenta curve) and the bore stirring term (Figure 5f). The effect of the downslope gravity term, which acted to mobilize sediment and increase the sheet flow layer thickness during the backwash (similar to a turbidity current) and counteracted sediment mobilization during the uprush, was significant due to the steep beach slope.

Focusing on a single swash event that begins at $t = 229s$, a large onshore-directed pressure gradient (Figure 5e, blue curve) and onshore-directed shear stress (enhanced by the fact that the boundary layer was not fully developed; Figure 5e, green curve) acted to mobilize sediment, while the downslope gravity counteracted sediment mobilization. However, the sudden increase of sheet flow layer thickness cannot be explained without introducing a bore stirring term (Figure 5f). Note the scale difference between Figures 5e and 5f and the fact that all forcing terms are scaled according to (18). During the backwash ($t = 237s$), sediment is mobilized by a combination of shear stress, pressure gradients and the downslope gravity.

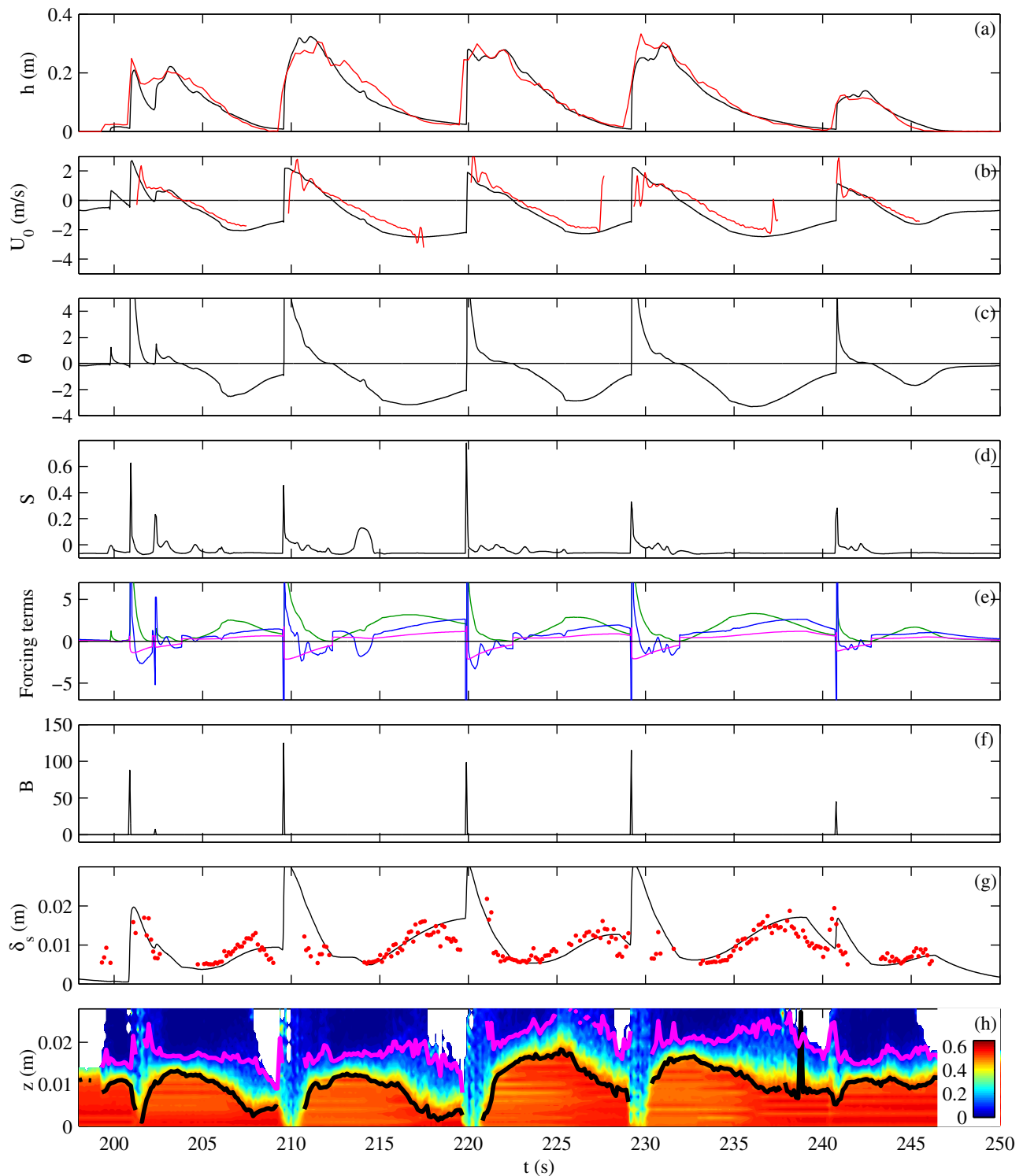


Figure 5. Time series excerpt of swash zone data group. Black curves indicate result from the (a, b) FUNwave and (g) sheet flow model; red curves and dots indicate measurements. (a) Water depth. (b) Cross-shore flow velocity. (c) Shields number. (d) *Sleath* number. (e) Mobilizing force terms: $\theta \text{ sign}(U_0)$: green curve; $YS \text{ sign}(U_0)$: blue curve; $-Y0.425C_0 \sin \beta \text{ sign}(U_0)$: magenta curve. (f) Bore stirring term. (g) Sheet flow layer thickness. (h) Sediment concentration measurements. Red tones indicate nonmoving sediment bed; blue tones indicate water column. Magenta and black curves indicate top and bottom of the sheet flow layer following Lanckriet et al. [2014], respectively.

The effect of the bore term is further demonstrated by running the sheet flow model with the bore stirring term deactivated, by setting $C_3 = 0$ (Figure 6d). The pressure gradient and shear stress were not sufficient to create the large sheet flow layer thicknesses observed during the uprush. The difference in predicted δ_s

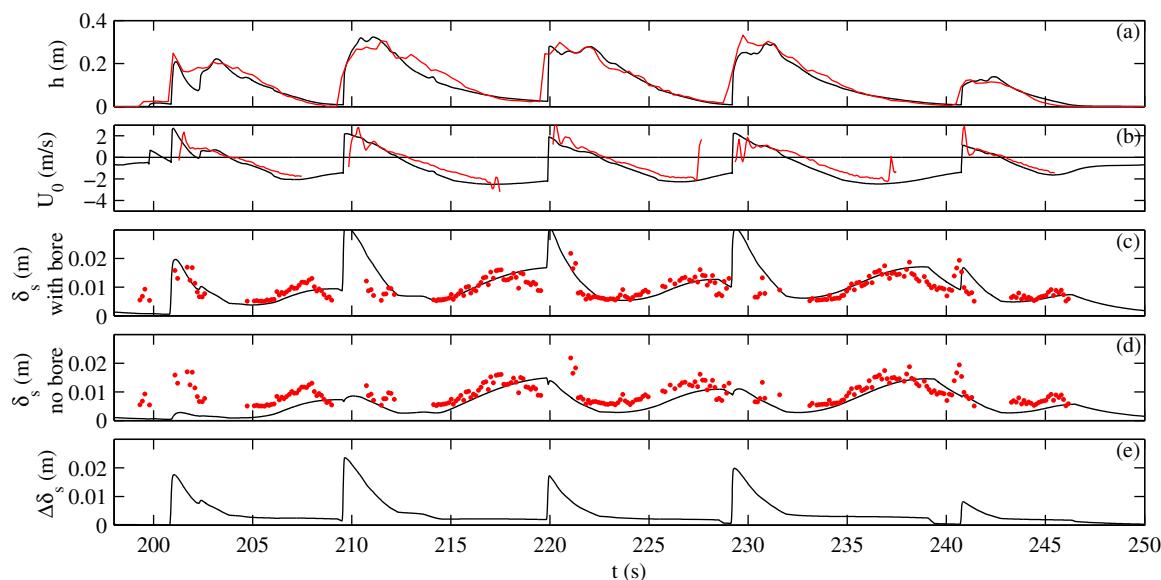


Figure 6. Time series excerpt highlighting effect of bore term. Black curves indicate result from the (a, b) FUNwave and (c, d) sheet flow model; red curves and dots indicate measurements. (a) Water depth. (b) Cross-shore flow velocity. (c) Sheet flow layer thickness—model prediction including bore term. (d) Sheet flow layer thickness—model prediction without bore term. (e) Difference between sheet flow layer thickness model predictions with and without bore term.

due to bore turbulence was up to 0.02 m (Figure 6e). Efforts to recalibrate the model without the bore stirring term were not sufficient to correct for the lack of a bore stirring term.

5. Discussion

5.1. Model Development

A new model was developed that predicts sheet flow layer thickness time series under generalized forcing conditions. The model is semianalytic because it consists of 2 coupled ODEs that are solved numerically given an input time series of the hydrodynamic forcing, represented by $U_0(t)$, $\frac{\partial p(t)}{\partial x}$ and $B(t)$. Several physical effects are included in the model, including boundary layer growth (resulting in increased friction factors at the beginning of uprush), pressure gradients (thus unifying sheet flow and plug flow formulations), and two-way interaction between bed roughness, sheet flow layer thickness and shear stress. The right-hand side of equation (13) consists of a force balance between four bed-parallel (quasi-horizontal) forces, whereas the left-hand side contains the (vertical) change in sheet flow layer thickness and the sediment fall velocity. The relationship between horizontal forces and vertical movement is similar to dilatancy observed in granular materials [Reynolds, 1885].

Due to the simplicity of the model, several physical processes were not included:

1. The boundary layer integral method cannot predict nonzero shear stresses at flow reversal or shear stresses in the direction opposite the free-stream flow. These were observed in the oscillatory flow tunnel data set (Figure 4, plots 21–23). Stresses opposite the free-stream flow likely occur in the swash zone as well. However, the effect of these phase lags is expected to decrease as the swash period increases.
2. The effects of boundary layer streaming [Dohmen-Janssen and Hanes, 2002; Nielsen, 2006; Yu *et al.*, 2010] and of groundwater in/exfiltration [Turner and Masselink, 1998], which affect net sediment transport, are not included in the model. For example, groundwater infiltration induces a net downward force on sediment grains (counteracting sediment mobilization) but also decreases the boundary thickness, increasing the shear stress (enhancing sediment mobilization) [Butt *et al.*, 2001]. Boundary layer streaming did not occur in the oscillatory flow tunnel experiments and no significant groundwater flow occurred in either the oscillatory flow tunnel or the swash zone experiments, but both processes could conceivably be incorporated into the model.
3. The model implicitly assumes that the sheet flow layer moves in the direction of the free-stream flow velocity U_0 at all times. This means that the pressure gradient acts as a mobilizing force when it acts in

the direction of the flow and as a resisting force when it acts against the direction of the flow. This assumption also leads to discontinuities in the pressure gradient forcing term at flow reversal (Figure 4, plots 41–49, blue curve).

4. The model does not include the sediment exchange between the suspended sediment in the water column and the sheet flow layer. For example, when hydrodynamic forcing decreases around flow reversal, sediment settles from the suspended load layer into the sheet flow layer which may delay the decrease in sheet flow layer thickness.
5. The effect of a variable friction factor (due to boundary layer growth and variable bottom roughness) on the bulk flow (modeled by FUNwave) was not resolved because FUNwave and the sheet flow model were not two-way coupled. The use of a constant friction factor in the current FUNwave model likely caused overprediction of $\delta_s(t)$ during the last stages of the backwash (Figure 5, $t = 215 - 220$ s). During the backwash, large sheet flow layer thicknesses result in a large bottom roughness K_n (equation (22)) and thus an enlarged friction factor. When this enlarged backwash friction factor would be incorporated in the bulk flow model, it would act to reduce the maximum backwash velocity, shear stress and $\delta_s(t)$. *Briganti et al.* [2011] coupled the momentum integral method (equation (21)) to a nonlinear shallow water model similar to FUNwave. Adding the $\delta_s(t)$ model would also be possible.

The pressure gradient force in (13) was assumed to apply to the entire sheet flow layer thickness $\delta_s(t)$, in accordance with the derivation by *Sleath* [1999]. In contrast, [*Othman et al.*, 2014] propose that the pressure gradient force must be multiplied by the grain diameter d , instead of the sheet flow layer thickness $\delta_s(t)$. Using d instead of $\delta_s(t)$ may be more applicable to pure bedload motion, where the mobile bed layer thickness is approximately equal to d , rather than to sheet flow, and would drastically reduce the importance of the pressure gradient forcing term.

The model was developed to predict $\delta_s(t)$ and not the time-dependent net sheet flow sediment transport. Measurements of the sediment transport are not yet available from swash zone experiments because of the difficulty in measuring flow velocity in the swash-zone sheet flow layer. Measurements of the time-dependent sediment flux are available from oscillatory flow tunnel experiments [e.g., *McLean et al.*, 2001; *O'Donoghue and Wright*, 2004b; *Hurther and Thorne*, 2011]. The model presented here could be modified to predict the net sediment transport if a suitable formulation for the velocity in the sheet flow layer would be implemented. However, the model would still be of limited use for practical applications because of the computation time needed to solve the ODEs and because errors in the sediment transport prediction would accumulate over time [*Masselink et al.*, 2009]. This model was instead developed to gain understanding of the different forcing mechanisms for sheet flow in the swash zone, which can then be used to improve practical parameterizations for the net sediment transport.

5.2. Model-Data Comparison

Given its simplicity, the model provided a good description of shear stress and sheet flow layer thickness for a range of different realistic wave shapes and grain sizes. The model skill can be assessed using the Brier skill score (equation (A4)). For the oscillatory flow tunnel data set, the new model (with two calibration coefficients C_1 and C_2) was 62% more accurate (BSS = 0.62, Table 2) at predicting the sheet flow layer than a prediction based on only the flow velocity squared (equation (A6)), which has one calibration coefficient. One possible source of error between modeled and measured sheet flow layer thicknesses in the oscillatory flow tunnel data group is methodological differences (e.g., a slightly different definition for the top and bottom of the sheet flow layer) in the two experimental studies that make up the data group. In addition, *Malarkey et al.* [2009] investigated the *O'Donoghue and Wright* [2004a, 2004b] data set (cases MA5010, MA7515, CA5010 and CA7515 in Figure 4) and found an inconsistency in the measurements for the cases CA5010 and CA7515, possibly due to horizontal nonuniformity in the oscillatory flow tunnel or due to the measurement uncertainty in the sediment concentration measurements. This inconsistency in the measurements led to an overprediction of δ_s by their model. The overprediction of δ_s for the cases CA5010 and CA7515 by the model proposed here is therefore likely due (in part) to the measurement inconsistencies described by *Malarkey et al.* [2009] as well.

The model by *Malarkey et al.* [2003, 2009] also consisted of two layers (the sheet flow layer and the upper water column). They modeled the sheet flow layer with an empirical parameterization based on sinusoidal

waveform measurements (which could be considered less complex than the force-based sheet flow layer model proposed here), and calculated the shear stresses in the upper water column using a $k-\epsilon$ turbulence closure model (more complex than the model proposed here). Detailed information on the model-data agreement by the *Malarkey et al.* [2003, 2009] was not available but the performance of the two models appears similar.

For the swash zone data group, the model (with three calibration coefficients C_1 - C_3) was 38% more accurate (BSS = 0.38, Table 2) than a prediction based on the flow velocity squared. It may seem counterintuitive that the model has a lower BSS for the swash zone data group (with three calibration coefficients) than for the oscillatory flow tunnel data group (with two calibration coefficients). However, an oscillatory flow tunnel is a much more controlled environment for generating sheet flow than a swash zone created in a large scale wave flume. An additional indication that the model captures the physics of the sheet flow layer is that the calibration factor C_2 was $O(1)$ for both the oscillatory flow tunnel and the swash zone data sets.

It is noted that the proposed model has more free parameters than the baseline model (equation (A6)) so that a certain improvement in model skill is expected. The baseline model (A6) was chosen because it has been used in past studies to predict δ_s [*Sumer et al.*, 1996; *Dohmen-Janssen and Hanes*, 2005]. Baseline models with the same number of free parameters as the proposed model were also tested, such as a linear (2 free parameters) or a quadratic (3 free parameters) polynomial expansion of U_0^2 :

$$\begin{aligned} \delta_s &= A + BU_0^2 && \text{Oscillatory flow tunnel data group} \\ \delta_s &= A + BU_0^2 + CU_0^4 && \text{Swash zone data group} \end{aligned} \tag{26}$$

However, these polynomials contain a constant term A , meaning that they predict a nonzero δ_s even for zero flow velocity, which is nonphysical. The baseline models in (26) have a lower RMSE than the proposed model but this is due to the constant term. In the oscillatory flow tunnel data set, $\delta_s(t)$ varies in the relatively narrow range of approx. 3–8 mm, meaning that a constant term alone already provides a reasonable first estimate of $\delta_s(t)$, without providing any meaningful information on the physical mechanisms involved. In the swash zone, $\delta_s(t)$ values less than or equal to 5 mm were not included because they were not resolved by the CCP sensor, meaning that a model with a constant term is not penalized for predicting non-zero sheet flow layer thickness when the real $\delta_s(t)$ is (nearly) zero. In conclusion, even though the proposed model (which is based on physical arguments) has a higher RMSE, it is still more useful to investigate the mechanisms of sheet flow than the polynomial baseline models (26), since the latter have a nonphysical basis and a more limited range of application.

5.3. Implications for Swash Zone Sediment Transport

The maximum Sleath number in the oscillatory flow tunnel data set was $S = 0.12$, occurring in cases MA5010 and CA5100, which is slightly larger than the criterion for plug flow proposed by *Foster et al.* [2006] ($S > 0.1$) but smaller than the criterion proposed by *Sleath* [1999] ($S > 0.29$). Around flow reversal, the effect of the pressure gradient was larger than the shear stress. However, the shear stress increased rapidly and became larger than the maximum pressure gradient force during the crest of the wave (Figure 4, plot 46). For all 9 waveforms, the shear stress was the dominant forcing mechanism. The pressure gradient provided a secondary effect. The notion that the pressure gradient effect was secondary to the shear stress is in agreement with findings from a discrete particle model by *Calantoni and Puleo* [2006].

In the swash zone data sets, large $\delta_s(t)$ values were observed at the beginning stages of the uprush (Figure 5, $t = 210$ s, 220 s, 230 s). The boundary layer integral method correctly predicted increased shear stresses because of the small boundary layer thickness upon bore arrival (Figure 5b). The maximum Sleath number in the swash zone data set was $S = 0.78$ occurring at $t = 219.9$ s, although the exact magnitude of the pressure gradient peak is uncertain because of the $\frac{\partial p}{\partial x}$ estimation method (equation (25)). S was thus larger than the criterion for plug flow, meaning that a combination of sheet flow and plug flow could have occurred during the beginning stages of the uprush. However, the pressure gradient and shear stress forces were insufficient to cause the rapid $\delta_s(t)$ increase during the beginning stages of the uprush in the swash zone data set (Figure 6). It is clear that another forcing mechanism must be responsible for this intense sediment mobilization, and bore-generated turbulence is a likely candidate [*Puleo et al.*, 2000; *Butt et al.*, 2004; *Jackson et al.*, 2004; *Aagaard and Hughes*, 2006]. From measurements of the near-bed turbulence dissipation rate ϵ in the swash zone of a natural beach, *Langkriet and Puleo* [2013] observed that ϵ was largest immediately

following bore arrival and then decayed rapidly. The sheet flow layer thickness model presented here, which predicted $\delta_s(t)$ correctly under pressure gradients and shear stress in the oscillatory water tunnel data set, could only predict $\delta_s(t)$ in the swash zone when an ad hoc formulation was added to incorporate the effect of bore-generated turbulence. More research is needed to investigate the effect of (bore-generated) turbulence on the sheet flow layer in greater detail, but the results presented in this paper indicate that bore turbulence is more important than pressure gradients for near-bed sediment transport in the swash zone during the initial uprush phase.

6. Conclusions

A new semianalytical model was developed to predict time-dependent sheet flow layer thickness under generalized forcing conditions and to investigate sheet flow in the swash zone. The model consists of two coupled ordinary differential equations that are solved numerically given an input time series of the hydrodynamic forcing.

Model validation was performed for two data groups. First, the model was validated against two experimental studies of sheet flow conducted in oscillatory flow tunnels, which are representative for conditions in the shoaling and outer surf zone where breaking wave-generated turbulence does not reach the near-bed sediment. Good agreement was observed between modeled and measured sheet flow layer thickness and shear stress, with a 62% improvement in model skill compared to a simple model based on the flow velocity squared. Sheet flow was generated by a combination of shear stresses and pressure gradients, with shear stress being the dominant mobilization mechanism.

The sheet flow model was also compared to a sheet flow layer thickness time series measured in the swash zone of a prototype-scale laboratory experiment. During the backwash, sheet flow was generated by a combination of shear stress, pressure gradients and downslope gravity. During the uprush, these three forcing mechanisms were not sufficient to explain the observed rapid increase in sheet flow layer thickness. This intense sheet flow is most likely attributed to bore-generated turbulence. Good agreement was found with a model that incorporated bore turbulence, demonstrated by a 31% improvement in model skill over a model based on flow velocity squared.

Appendix A: Model Calibration

The three calibration factors $C_1 - C_3$ were determined to maximize the model skill in predicting the measured $\delta_s(t)$ time series. Several different metrics exist that describe model skill [Roelvink and Reniers, 2012], including the (squared) Pearson product-moment correlation coefficient, r^2 , the root mean square error (RMSE), the coefficient of determination, R^2 and the Brier Skill Score (BSS). The product-moment correlation coefficient is defined as:

$$r = \frac{\sum_{i=1}^n (f_i - \bar{f})(y_i - \bar{y})}{\sum_{i=1}^n (f_i - \bar{f}) \sum_{i=1}^n (y_i - \bar{y})} = \frac{\text{cov}(f, y)}{s(f)s(y)} \tag{A1}$$

where f_i are model predictions of a certain parameter (in this case δ_s), y_i are observations of the same parameter, and the overbar signifies a sample mean. $\text{cov}(f, y)$ is the sample covariance between predictions and observations and $s(f)$ and $s(y)$ are the sample standard deviations of the model predictions and observations, respectively. The correlation coefficient is a measure of how model and measurements covary, but it is not sensitive to a bias or error in scale in the model.

The Root Mean Square Error (RMSE), the coefficient of determination R^2 , and the Brier Skill Score (BSS) are defined as:

$$\text{RMSE} = \sqrt{\sum_{i=1}^n (f_i - y_i)^2} \tag{A2}$$

$$R^2 = 1 - \frac{\sum_{i=1}^n (f_i - y_i)^2}{\sum_{i=1}^n (y_i - \bar{y})^2}, \tag{A3}$$

Table A1. Calibration Coefficients and Model Skill Statistics for the Sheet Flow Layer Thickness Model, Calibrated Using Different Choices of the Optimization Parameters (α_1, α_2)^a

α_1	α_2	RMSE (mm)	r^2	R^2	BSS	C_1	C_2	C_3
<i>Oscillatory Flow Tunnel Data Set</i>								
<i>2/3</i>	<i>1/3</i>	1.70	0.34	0.15	0.62	41.65	0.57	
1/2	1/2	1.68	0.31	0.16	0.63	46.44	0.57	
0	1	1.65	0.26	0.19	0.64	62.18	0.57	
<i>Swash Zone Data Set Complete Time Series</i>								
<i>2/3</i>	<i>1/3</i>	4.15	0.33	-0.95	0.32	49.56	1.71	317.36
1/2	1/2	4.06	0.29	-0.86	0.35	63.87	1.74	362.68
0	1	4.02	0.25	-0.82	0.37	83.57	1.82	417.73
<i>Excluding Swash Events < 0.07 m</i>								
<i>2/3</i>	<i>1/3</i>	3.71	0.38	-0.45	0.38	49.56	1.71	317.36
1/2	1/2	3.60	0.33	-0.37	0.41	63.87	1.74	362.68
0	1	3.57	0.28	-0.35	0.42	83.57	1.82	417.73

^aVariables are italicized.

$$BSS = 1 - \frac{\sum_{i=1}^n (f_i - y_i)^2}{\sum_{i=1}^n (b_i - y_i)^2}, \tag{A4}$$

where b_i are predictions by a baseline model. Both $(1 - R^2)$ and $(1 - BSS)$ are proportional to the mean square error (MSE, the square of the RMSE), meaning that calibrating a model by minimizing RMSE is equivalent to maximizing R^2 or BSS. In some cases, calibrating a model by minimizing the RMSE favors model predictions that underestimate observed variability [Arpe *et al.*, 1985; Murphy and Epstein, 1989]. In particular, when the sheet flow model was calibrated for the swash zone data set by minimizing the RMSE, the optimum calibration values included a spuriously large value for C_1 (indicative of the time lag of the sheet flow layer thickness) so that the predicted sheet flow layer thickness showed little temporal variability.

A calibration procedure was devised that combines the advantages of r^2 and R^2 and ensures that model predictions covary with the observations with minimal bias or scale error. The three calibration factors $C_1 - C_3$ were optimized to minimize *ERR* :

$$ERR = \alpha_1 (1 - r^2) + \alpha_2 (1 - R^2), \tag{A5}$$

where α_1 and α_2 are dimensionless optimization parameters that are chosen before calibration and indicate the relative importance of r^2 and R^2 in the model calibration. Model calibrations were performed for 3 different choices of (α_1, α_2) and results are summarized in Table A1. Choosing $\alpha_1 = 2/3, \alpha_2 = 1/3$ instead of $\alpha_1 = 0, \alpha_2 = 1$ (purely minimizing the RMSE), led to a significant improvement in r^2 at the cost of a small increase in the RMSE for both data sets. The coefficients $\alpha_1 = 2/3, \alpha_2 = 1/3$ were therefore chosen to calibrate the model.

The Brier Skill Score (equation (A4)) was calculated using the following baseline model for the sheet flow layer thickness:

$$\delta_s = m_1 U^2, \tag{A6}$$

where m_1 is a fitting coefficient that was determined by linear regression for each data group. This model is equivalent to Wilson's [1987] model for stationary sheet flow (equation (1)) when τ_b is calculated as

$$\tau_b = \frac{1}{2} \rho f U^2 \tag{A7}$$

with a constant friction factor f . It is also equivalent to a linear relationship between sheet flow layer thickness and mobility number, for which good agreement was observed during quasi-steady backwash [Lanckriet *et al.*, 2014], and to the notion that the amount of sediment mobilized in the near-bed layer is proportional to U^2 , which is included in many coastal sediment transport models [Bagnold, 1966; Bailard, 1981]. The BSS (Tables 2 and A1) thus quantifies the improvement of the time-dependent sheet flow model over the stationary model of Wilson [1987].

Acknowledgments

This work was supported by National Science Foundation (grants OCE-0845004 and OCE-1332703) and the University of Delaware. The swash-zone data set was collected during the BARDEX II project that was supported by the 7th Framework Programme of the European Community through the Integrating Activity HYDRALAB IV, contract 261520. The authors wish to thank Tom O'Donoghue and Gerben Ruessink for sharing their oscillatory flow tunnel data sets, as well as three anonymous reviewers for their constructive remarks that greatly improved this contribution.

References

- Aagaard, T., and M. G. Hughes (2006), Sediment suspension and turbulence in the swash zone of dissipative beaches, *Mar. Geol.*, 228(1–4), 117–135, doi:10.1016/j.margeo.2006.01.003.
- Ahmed, A. S. M., and S. Sato (2003), A sheetflow transport model for asymmetric oscillatory flows: Part II: Mixed grain size sediments, *Coastal Eng. J.*, 45(03), 339–361, doi:10.1142/S0578563403000798.
- Amoudry, L., T.-J. Hsu, and P. L.-F. Liu (2008), Two-phase model for sand transport in sheet flow regime, *J. Geophys. Res.*, 113, C03011, doi:10.1029/2007JC004179.
- Arpe, B. K., A. Hollingsworth, M. S. Tracton, A. C. Lorenc, S. Uppala, and P. Kållberg (1985), The response of numerical weather prediction systems to fgge level iib data. Part II: Forecast verifications and implications for predictability, *Q. J. R. Meteorol. Soc.*, 111(467), 67–101, doi:10.1002/qj.49711146703.
- Bagnold, R. A. (1956), The flow of cohesionless grains in fluids, *Proc. R. Soc. London, Ser. A.*, 249(964), 235–297.
- Bagnold, R. A. (1966), An approach to the sediment transport problem from general physics, *U.S. Geol. Surv. Prof. Pap.*, 422-I, U.S. Gov. Print. Off., Washington, D. C.
- Bailard, J. A. (1981), An energetics total load sediment transport model for a plane sloping beach, *J. Geophys. Res.*, 86(C11), 10938–10954, doi:10.1029/JC086iC11p10938.
- Bakhtyar, R., A. Yeganeh-Bakhtiyari, D. A. Barry, and A. Ghaheri (2009), Two-phase hydrodynamic and sediment transport modeling of wave-generated sheet flow, *Adv. Water Resour.*, 32(8), 1267–1283, doi:10.1016/j.advwatres.2009.05.002.
- Bakhtyar, R., D. A. Barry, A. Yeganeh-Bakhtiyari, L. Li, J.-Y. Parlange, and G. C. Sander (2010), Numerical simulation of two-phase flow for sediment transport in the inner-surf and swash zones, *Adv. Water Resour.*, 33(3), 277–290, doi:10.1016/j.advwatres.2009.12.004.
- Baldock, T. E., and P. Holmes (1997), Swash hydrodynamics on a steep beach, in *Coastal Dynamics '97*, edited by E. B. Thornton, pp. 784–793, ASCE, N. Y.
- Baldock, T. E., and M. G. Hughes (2006), Field observations of instantaneous water slopes and horizontal pressure gradients in the swash-zone, *Cont. Shelf Res.*, 26(5), 574–588, doi:10.1016/j.csr.2006.02.003.
- Baldock, T. E., R. Grayson, B. Torr, and H. E. Power (2014), Flow convergence at the tip and edges of a viscous swash front—Experimental and analytical modeling, *Coastal Eng.*, 88, 123–130, doi:10.1016/j.coastaleng.2014.02.008.
- Barnes, M. P., and T. E. Baldock (2010), A Lagrangian model for boundary layer growth and bed shear stress in the swash zone, *Coastal Eng.*, 57(4), 385–396, doi:10.1016/j.coastaleng.2009.11.009.
- Battjes, J. A., and J. P. F. M. Janssen (1978), Energy loss and set-up due to breaking of random waves, *Int. Conf. Coastal Eng.*, 1(16), 569–587, doi:10.9753/icce.v16.
- Blenkinsopp, C. E., I. L. Turner, G. Masselink, and P. E. Russell (2010), Validation of volume continuity method for estimation of cross-shore swash flow velocity, *Coastal Eng.*, 57(10), 953–958, doi:10.1016/j.coastaleng.2010.05.005.
- Briganti, R., N. Dodd, D. Pokrajac, and T. O'Donoghue (2011), Non linear shallow water modelling of bore-driven swash: Description of the bottom boundary layer, *Coastal Eng.*, 58(6), 463–477, doi:10.1016/j.coastaleng.2011.01.004.
- Butt, T., and P. Russell (1999), Suspended sediment transport mechanisms in high-energy swash, *Mar. Geol.*, 161(2–4), 361–375, doi:10.1016/S0025-3227(99)00043-2.
- Butt, T., P. Russell, and I. Turner (2001), The influence of swash infiltration—exfiltration on beach face sediment transport: Onshore or offshore?, *Coastal Eng.*, 42(1), 35–52, doi:10.1016/S0378-3839(00)00046-6.
- Butt, T., P. Russell, J. Puleo, J. Miles, and G. Masselink (2004), The influence of bore turbulence on sediment transport in the swash and inner surf zones, *Cont. Shelf Res.*, 24(7–8), 757–771, doi:10.1016/j.csr.2004.02.002.
- Calantoni, J., and J. A. Puleo (2006), Role of pressure gradients in sheet flow of coarse sediments under sawtooth waves, *J. Geophys. Res.*, 111, C01010, doi:10.1029/2005JC002875.
- Camenen, B., and M. Larson (2006), Phase-lag effects in sheet flow transport, *Coastal Eng.*, 53(5–6), 531–542, doi:10.1016/j.coastaleng.2005.12.003.
- Chassagneux, F. X., and D. Hurther (2014), Wave bottom boundary layer processes below irregular surfzone breaking waves with light-weight sheet flow particle transport, *J. Geophys. Res. Oceans*, 119, 1668–1690, doi:10.1002/2013JC009338.
- Chen, X., Y. Li, X. Niu, D. Chen, and X. Yu (2011), A two-phase approach to wave-induced sediment transport under sheet flow conditions, *Coastal Eng.*, 58(11), 1072–1088, doi:10.1016/j.coastaleng.2011.06.003.
- Clarke, S., N. Dodd, and J. Damgaard (2004), Modeling flow in and above a porous beach, *J. Waterw. Port Coastal Ocean Eng.*, 130(5), 223–233, doi:10.1061/(ASCE)0733-950X(2004)130:5(223).
- da Silva, P. A., A. Temperville, and F. Seabra Santos (2006), Sand transport under combined current and wave conditions: A semi-unsteady, practical model, *Coastal Eng.*, 53(11), 897–913, doi:10.1016/j.coastaleng.2006.06.010.
- Dibajnia, M., and A. Watanabe (1998), Transport rate under irregular sheet flow conditions, *Coastal Eng.*, 35(3), 167–183, doi:10.1016/S0378-3839(98)00034-9.
- Dohmen-Janssen, C. M., and D. M. Hanes (2002), Sheet flow dynamics under monochromatic nonbreaking waves, *J. Geophys. Res.*, 107(C10), 3149, doi:10.1029/2001JC001045.
- Dohmen-Janssen, C. M., and D. M. Hanes (2005), Sheet flow and suspended sediment due to wave groups in a large wave flume, *Cont. Shelf Res.*, 25(3), 333–347, doi:10.1016/j.csr.2004.10.009.
- Dohmen-Janssen, C. M., W. N. Hassan, and J. S. Ribberink (2001), Mobile-bed effects in oscillatory sheet flow, *J. Geophys. Res.*, 106(C11), 27,103–27,115, doi:10.1029/2000JC000513.
- Dong, L. P., S. Sato, and H. Liu (2013), A sheetflow sediment transport model for skewed-asymmetric waves combined with strong opposite currents, *Coastal Eng.*, 71, 87–101, doi:10.1016/j.coastaleng.2012.08.004.
- Drake, T. G., and J. Calantoni (2001), Discrete particle model for sheet flow sediment transport in the nearshore, *J. Geophys. Res.*, 106(C9), 19,859–19,868, doi:10.1029/2000JC000611.
- Foster, D. L., A. J. Bowen, R. A. Holman, and P. Nattoo (2006), Field evidence of pressure gradient induced incipient motion, *J. Geophys. Res.*, 111, C05004, doi:10.1029/2004JC002863.
- Frank, D., D. Foster, P. Chou, Y.-M. Kao, I. M. Sou, and J. Calantoni (2014), Development and evaluation of an autonomous sensor for the observation of sediment motion, *J. Atmos. Oceanic Technol.*, 31, 1012–1019, doi:10.1175/JTECH-D-13-00180.1.
- Fredsøe, J. (1984), Turbulent boundary layer in wave-current motion, *J. Hydraul. Eng.*, 110(8), 1103–1120.
- Fredsøe, J., and R. Deigaard (1992), *Mechanics of Coastal Sediment Transport*, *Adv. Ser. Ocean Eng.*, vol. 3, 369 pp., World Sci., Singapore.
- Gonzalez-Rodriguez, D., and O. S. Madsen (2007), Seabed shear stress and bedload transport due to asymmetric and skewed waves, *Coastal Eng.*, 54(12), 914–929, doi:10.1016/j.coastaleng.2007.06.004.

- Hoefel, F., and S. Elgar (2003), Wave-induced sediment transport and sandbar migration, *Science*, 299(5614), 1885–1887.
- Horikawa, K., A. Watanabe, and S. Katori (1982), Sediment transport under sheet flow conditions, in *Proceedings of 18th International Conference on Coastal Engineering*, edited by B. L. Edge, pp. 1335–1352, Am. Soc. of Civ. Eng., N. Y.
- Horn, D. P., and T. Mason (1994), Swash zone sediment transport modes, *Mar. Geol.*, 120(3–4), 309–325, doi:10.1016/0025-3227(94)90064-7.
- Houser, C., and G. Barrett (2009), Bed elevation changes in the upper-swash zone, *J. Coastal Res.*, 56, 64–68.
- Hsu, T.-J., J. T. Jenkins, and P. L.-F. Liu (2004), On two-phase sediment transport: Sheet flow of massive particles, *Proc. R. Soc. London, Ser. A*, 460(2048), 2223–2250, doi:10.1098/rspa.2003.1273.
- Hurther, D., and P. D. Thorne (2011), Suspension and near-bed load sediment transport processes above a migrating, sand-rippled bed under shoaling waves, *J. Geophys. Res.*, 116, C07001, doi:10.1029/2010JC006774.
- Jackson, N. L., G. Masselink, and K. F. Nordstrom (2004), The role of bore collapse and local shear stresses on the spatial distribution of sediment load in the uprush of an intermediate-state beach, *Mar. Geol.*, 203(1–2), 109–118, doi:10.1016/S0025-3227(03)00328-1.
- Karambas, T. (2003), Modelling of infiltration-exfiltration effects of cross-shore sediment transport in the swash zone, *Coastal Eng. J.*, 45(1), 63–82, doi:10.1142/S057856340300066X.
- Lanckriet, T., and J. A. Puleo (2013), Near-bed turbulence dissipation measurements in the inner surf and swash zone, *J. Geophys. Res., Oceans*, 118, 6634–6647, doi:10.1002/2013JC009251.
- Lanckriet, T., J. A. Puleo, and N. Waite (2013), A conductivity concentration profiler for sheet flow sediment transport, *IEEE J. Oceanic Eng.*, 38(1), 55–70, doi:10.1109/JOE.2012.2222791.
- Lanckriet, T., J. Puleo, G. Masselink, I. Turner, D. Conley, C. Blenkinsopp, and P. Russell (2014), Comprehensive field study of swash-zone processes. II: Sheet flow sediment concentrations during quasi-steady backwash, *J. Waterw. Port Coastal Ocean Eng.*, 140(1), 29–42, doi:10.1061/(ASCE)WW.1943-5460.0000209.
- Malarkey, J., A. Davies, and Z. Li (2003), A simple model of unsteady sheet-flow sediment transport, *Coastal Eng.*, 48(3), 171–188, doi:10.1016/S0378-3839(03)00025-5.
- Malarkey, J., S. Pan, M. Li, T. O'Donoghue, A. G. Davies, and B. A. O'Connor (2009), Modelling and observation of oscillatory sheet-flow sediment transport, *Ocean Eng.*, 36(11), 873–890, doi:10.1016/j.oceaneng.2009.05.003.
- Masselink, G., D. Evans, M. G. Hughes, and P. Russell (2005), Suspended sediment transport in the swash zone of a dissipative beach, *Mar. Geol.*, 216(3), 169–189, doi:10.1016/j.margeo.2005.02.017.
- Masselink, G., P. Russell, I. Turner, and C. Blenkinsopp (2009), Net sediment transport and morphological change in the swash zone of a high-energy sandy beach from swash event to tidal cycle time scales, *Mar. Geol.*, 267(1–2), 18–35, doi:10.1016/j.margeo.2009.09.003.
- McLean, S. R., J. S. Ribberink, C. M. Dohmen-Janssen, and W. N. Hassan (2001), Sand transport in oscillatory sheet flow with mean current, *J. Waterw. Port Coastal Ocean Eng.*, 127(3), 141–151, doi:10.1061/(ASCE)0733-950X(2001)127:3(141).
- Murphy, A. H., and E. S. Epstein (1989), Skill scores and correlation coefficients in model verification, *Mon. Weather Rev.*, 117(3), 572–582, doi:10.1175/1520-0493(1989)117<0572:SSACCI>2.0.CO;2.
- Nielsen, P. (2006), Sheet flow sediment transport under waves with acceleration skewness and boundary layer streaming, *Coastal Eng.*, 53(9), 749–758, doi:10.1016/j.coastaleng.2006.03.006.
- O'Donoghue, T., and S. Wright (2004a), Concentrations in oscillatory sheet flow for well sorted and graded sands, *Coastal Eng.*, 50(3), 117–138, doi:10.1016/j.coastaleng.2003.09.004.
- O'Donoghue, T., and S. Wright (2004b), Flow tunnel measurements of velocities and sand flux in oscillatory sheet flow for well-sorted and graded sands, *Coastal Eng.*, 51(11–12), 1163–1184, doi:10.1016/j.coastaleng.2004.08.001.
- Othman, I. K., T. E. Baldock, and D. P. Callaghan (2014), Measurement and modelling of the influence of grain size and pressure gradient on swash uprush sediment transport, *Coastal Eng.*, 83, 1–14, doi:10.1016/j.coastaleng.2013.09.001.
- Puleo, J. A., R. A. Beach, R. A. Holman, and J. S. Allen (2000), Swash zone sediment suspension and transport and the importance of bore-generated turbulence, *J. Geophys. Res.*, 105(C7), 17,021–17,044, doi:10.1029/2000JC900024.
- Puleo, J. A., K. T. Holland, N. G. Plant, D. N. Slinn, and D. M. Hanes (2003), Fluid acceleration effects on suspended sediment transport in the swash zone, *J. Geophys. Res.*, 108(C11), 3350, doi:10.1029/2003JC001943.
- Puleo, J. A., A. Farhadzadeh, and N. Kobayashi (2007), Numerical simulation of swash zone fluid accelerations, *J. Geophys. Res.*, 112, C07007, doi:10.1029/2006JC004084.
- Puleo, J. A., T. Lanckriet, and C. Blenkinsopp (2014a), Bed level fluctuations in the inner surf and swash zone of a dissipative beach, *Mar. Geol.*, 349, 99–112, doi:10.1016/j.margeo.2014.01.006.
- Puleo, J. A., et al. (2014b), Comprehensive field study of swash-zone processes. I: Experimental design with examples of hydrodynamic and sediment transport measurements, *J. Waterw. Port Coastal Ocean Eng.*, 140(1), 14–28, doi:10.1061/(ASCE)WW.1943-5460.0000210.
- Reynolds, O. (1885), On the dilatancy of media composed of rigid particles. With experimental illustrations, *Philos. Mag. Ser.*, 5 20, (127), 469–481, doi:10.1080/14786448508627791.
- Ribberink, J. S. (1998), Bed-load transport for steady flows and unsteady oscillatory flows, *Coastal Eng.*, 34(1–2), 59–82, doi:10.1016/S0378-3839(98)00013-1.
- Ribberink, J. S., and A. A. Al-Salem (1995), Sheet flow and suspension of sand in oscillatory boundary layers, *Coastal Eng.*, 25(3–4), 205–225, doi:10.1016/0378-3839(95)00003-T.
- Roelvink, D., and A. Reniers (2012), A Guide to Modeling Coastal Morphology, *Adv. Coastal Ocean Eng.*, 292 pp., World Sci., Singapore.
- Ruessink, B. G., H. Michallet, T. Abreu, F. Sancho, D. A. V. der A., J. J. V. der Werf, and P. A. Silva (2011), Observations of velocities, sand concentrations, and fluxes under velocity-asymmetric oscillatory flows, *J. Geophys. Res.*, 116, C03004, doi:10.1029/2010JC006443.
- Shampine, L., and M. Reichelt (1997), The MATLAB ODE suite, *SIAM J. Sci. Comput.*, 18(1), 1–22, doi:10.1137/S1064827594276424.
- Shi, F., J. T. Kirby, J. C. Harris, J. D. Geiman, and S. T. Grilli (2012), A high-order adaptive time-stepping TVD solver for Boussinesq modeling of breaking waves and coastal inundation, *Ocean Modell.*, 43–44, 36–51, doi:10.1016/j.ocemod.2011.12.004.
- Sleath, J. F. A. (1999), Conditions for plug formation in oscillatory flow, *Cont. Shelf Res.*, 19(13), 1643–1664, doi:10.1016/S0278-4343(98)00096-X.
- Sumer, B. M., A. Kozakiewicz, J. Fredsoe, and R. Deigaard (1996), Velocity and concentration profiles in sheet-flow layer of movable bed, *J. Hydraul. Eng.*, 122(10), 549–558, doi:10.1061/(ASCE)0733-9429(1996)122:10(549).
- Turner, I. L., and G. Masselink (1998), Swash infiltration-exfiltration and sediment transport, *J. Geophys. Res.*, 103(C13), 30,813–30,824, doi:10.1029/98JC02606.
- van der A, D. A., T. O'Donoghue, and J. S. Ribberink (2010), Measurements of sheet flow transport in acceleration-skewed oscillatory flow and comparison with practical formulations, *Coastal Eng.*, 57(3), 331–342, doi:10.1016/j.coastaleng.2009.11.006.
- van der A, D. A., J. S. Ribberink, J. J. van der Werf, T. O'Donoghue, R. H. Buijsrogge, and W. M. Kranenburg (2013), Practical sand transport formula for non-breaking waves and currents, *Coastal Eng.*, 76, 26–42, doi:10.1016/j.coastaleng.2013.01.007.

- Watanabe, A., and S. Sato (2004), A sheet-flow transport rate formula for asymmetric, forward-leaning waves and currents, in *Proceedings of 29th International Conference on Coastal Engineering*, edited by J. M. Smith, pp. 1703–1714, Am. Soc. of Civ. Eng., N. Y.
- Wilson, K. C. (1987), Analysis of bed-load motion at high shear stress, *J. Hydraul. Eng.*, *113*(1), 97–103, doi:10.1061/(ASCE)0733-9429(1987)113:1(97).
- Wilson, K. C. (1989), Mobile-bed friction at high shear stress, *J. Hydraul. Eng.*, *115*(6), 825–830.
- Yu, X., T.-J. Hsu, and D. M. Hanes (2010), Sediment transport under wave groups: Relative importance between nonlinear waveshape and nonlinear boundary layer streaming, *J. Geophys. Res.*, *115*, C02013, doi:10.1029/2009JC005348.